Acta Geotechnica (2022) 17:3407–3420
https://doi.org/10.1007/s11440-021-01432-1

RESEARCH PAPER

Calibrating and validating a soil constitutive model through conventional triaxial tests: an in-depth study on CSUH model

Binglong Zhu[1] · Zuyu Chen[2]

Received: 24 August 2021 / Accepted: 30 November 2021 / Published online: 3 January 2022

Abstract

This paper presents an approach for calibrating and validating a constitutive model via conventional triaxial tests. First, the consolidated drained triaxial compression test results are used for model calibration. The particle swarm optimization algorithm based on multiple adaptive strategies is then adopted to calibrate the best fitting parameters. Subsequently, the constitutive model is validated by considering its performance in modeling the consolidated undrained triaxial tests. The unified hardening model for clays and sands (CSUH model) proposed by Yao et al. (Comput Geotech 110:326–343, 2019. 10.1016/j.compgeo.2019.02.024) is considered. The results demonstrate that the CSUH model can well describe the dilatancy of clays and sands with different densities in both drained and undrained triaxial tests.

Keywords Cam-Clay model · Constitutive model · CSUH model · Dilatancy · Undrained test · Unified hardening model

Abbreviations

C_{ij}	The element of elastic matrix $\left[C_{ij}^{e}\right]$ or elastoplastic matrix $\left[C_{ij}^{ep}\right]$; i and j = 1, 2, 3
e	Current void ratio
e_0	Initial void ratio
e_{c0}	Void ratio on the critical state line (CSL) at p' = 0 kPa
E	Elastic modulus
H	Hardening parameter
m	Dilatancy parameter
M	Critical state stress ratio: slope of CSL in p'–q coordinates
M_c	Characteristic state stress ratio
M_f	Potential failure stress ratio
MRE	Assessment criteria: mean relative error
N	Void ratio of the asymptote of normal compression line (RNCL) at p' = 1 kPa in the $e \sim \ln p'$ coordinates
p'	Mean effective stress $p' = \frac{\sigma_1' + 2\sigma_3'}{3}$ in conventional compression test
p_x'	Intersection of current yield surface with the p'-axis
p_{x0}'	Initial value of p_x'
p_s	Compressive hardening parameter
p_y'	Intersection of plastic potential surface with the p'-axis
q	Deviatoric stress $q = \left(\sigma_1' - \sigma_3'\right)$ in conventional compression test
R	Assessment criteria: the determination coefficient
$\boldsymbol{R}$	Search area of exemplar X_i
u	Excess pore pressure
V_i	Velocity of exemplar
X_i	Exemplar or potential solution of the optimization problem
Z	The void ratio of the normal compression line (NCL) at p' = 1 kPa for sands in the $e \sim \ln p'$ coordinates
κ	Slope of the unloading line in the $e \sim \ln(p' + p_s)$ coordinates
λ	Slope of the NCL in the $e \sim \ln(p' + p_s)$ coordinates, is also the slope of the RNCL in the $e \sim \ln p'$ coordinates
η	Stress ratio $\eta = \frac{q}{p'}$
v	Poisson's ratio
χ	Critical state parameter
ξ	State variable describing the current density

✉ Zuyu Chen
chenzuyu@cashq.ac.cn

[1] School of Transportation Science and Engineering, Beihang University, Beijing 100191, China

[2] State Key Laboratory of Simulation and Regulation of Water Cycle in River Basin, Institute of Water Resources and Hydropower Research, No. 20, West Chegongzhuang Rd., Beijing 100048, China

ε_i	The maximum, medium and minimum principal strain when i = 1, 2, and 3, respectively
ε_v	Volumetric strain
ε_v^p	Plastic (unrecoverable) volumetric strain
σ_j'	The maximum, medium and minimum effective principal stress when j = 1, 2, 3, respectively
σ_{3i}'	Initial confine pressure in the shear stage
σ_c'	Pre-consolidation pressure
Λ	Total error: the average value of all individual error $MRE(X_i)$
$\Delta\varepsilon_i$	The ith principal strain increment, i = 1, 2, 3
$\Delta\sigma_j'$	The jth principal stress increment, j = 1, 2, 3

1 Introduction

Over the past few decades, numerous constitutive models for soils have been proposed, and more will be emerging in future [15, 36, 37]. When using a certain constitutive law in engineering design, one may be concerned with its calibration and validation.

1.1 Calibration of the parameters

A constitutive model normally involves a number of parameters. For example, the modified Cam-Clay (MCC) model includes five parameters related to the elastic and plastic behavior of soil [27–29, 32]. However, many of these parameters are derived from laboratory tests with particular stress paths that may not be representative for engineering problems. Moreover, the in situ stress history is often unknown, which hinders the use of laboratory tests.

One possible approach is to fit the constitutive model based on laboratory tests such as conventional triaxial and oedometer tests. In this case, some optimization methods can be used for model calibration. This fitting approach with optimization methods is not new. For instance, Pal et al. [23] used the genetic algorithm (GA) [10] to calibrate the parameters of the hierarchical single surface model. Sadoghi Yazdi et al. [31] adopted the particle swarm optimization (PSO) algorithm [11] to calibrate the parameters of the linear elastic-hardening plastic model with Drucker–Prager yield criterion. More applications can be found in references [1, 6, 16, 24, 54, 56].

1.2 Validation of the constitutive laws

The constitutive model should be validated by laboratory tests with various stress paths before engineering application. For example, Matsuoka et al. [20] developed a unified SMP model for clays and calibrated the parameters through conventional drained triaxial tests on normally consolidated Fujinomori clay (experimental data from Nakai and Matsuoka [22]). The calibrated parameters are then verified by independent test results, such as undrained triaxial compression and extension tests. More examples of model validation through independent test results can be found in the literature [4, 9, 12–14, 18, 21, 25, 26, 30, 34, 38, 39, 41, 44, 47, 50, 51].

Despite the aforementioned successes in the calibration and validation of constitutive laws, there still lacks standard methodologies. This manuscript presents an in-depth approach for calibrating and validating a constitutive model with conventional laboratory test results. Specifically, the unified hardening model for clays and sands (CSUH model) developed by Yao et al. [48] is considered. This constitutive model inherits the basic principles of the MCC model while extends its ability to model the mechanical behavior of both sands and clays. This manuscript reports the details of calibrating its eight basic parameters via consolidated drained triaxial compression (CD) tests. The calibrated parameters are further used to predict the consolidated undrained triaxial compression (CU) tests. This so-called "drained versus undrained" approach assures its universal applicability along various stress paths. The calibration solver and the related documentation and test cases can be found on the website: https://github.com/ChenZuyuIWHR/CSUH-BH.

In the remaining part of this manuscript, firstly, the theories of the CSUH model and its numerical implementation are detailed. Afterward, the particle swarm optimization algorithm based on multiple adaptive strategies (MAPSO) for model calibration is described. Finally, the model calibration and validation processes are presented, where the authors demonstrate the relative errors and determination coefficient of the predicted results.

2 The CSUH model

2.1 Model framework

It is well-known that state-dependent dilatancy and excess pore water pressure are two major challenges in constitutive modeling of soils [7, 8]. The original unified hardening (UH) model, proposed by Yao et al. [44–46] for overconsolidated clays based on the MCC model, is capable of characterizing these two issues by introducing a unified hardening law [50]. Because of this advantage, it is later extended for many kinds of soils, e.g., unsaturated soils [18] and structured soils [57], etc., and has gained popularity in many engineering practices [43, 52, 53, 55].

Table 1 Comparison between the CSUH and the MCC models

	Isotropic normal compression line: NCL	Plastic potential surface g	Yield surface f	Hardening parameter H
MCC	$e = N - \lambda \ln\left(\frac{p'}{1}\right)$	$g(p', q) = \ln\left(\left(1 + \frac{q^2}{M^2 p'^2}\right)p'\right) - \ln p'_y = 0$	$f(p', q, H) = \ln\left(\left(1 + \frac{q^2}{M^2 p'^2}\right)p'\right) - \ln p'_{x0} - \frac{1}{c_p}H = 0$	$H = \int d\varepsilon_v^p$
CSUH	$e = Z - \lambda \ln\left(\frac{p'+p_s}{1+p_s}\right)$	$g(p', q) = \ln\left(\left(1 + \frac{q^2}{M_c^2 p'^2}\right)p'\right) - \ln p'_y = 0$	$f = \ln\left(\left(1 + \frac{(1+\chi)q^2}{M^2 p'^2 - \chi q^2}\right)p' + p_s\right) - \ln\left(p'_{x0} + p_s\right) - \frac{1}{c_p}H = 0$	$H = \int \frac{M_f^4 - \eta^4}{M_c^4 - \eta^4} d\varepsilon_v^p$
	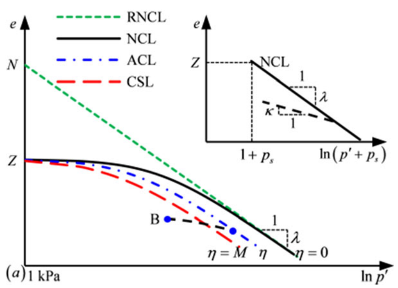	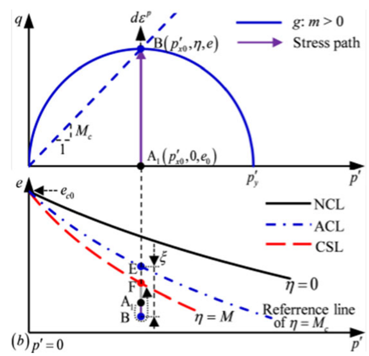	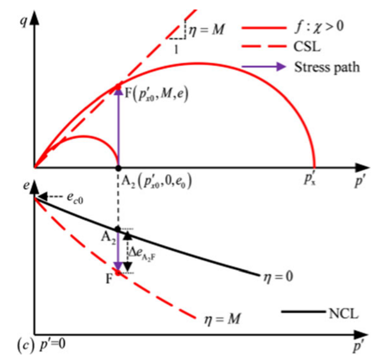	

A_1 and A_2 are the initial state points; E is the density reference point for current point B; F is the critical state point

Table 2 The basic parameters and intermediate variables of the CSUH model

Symbol	Aspects	Description
Basic parameters		
M	Yielding	Slope of CSL in $p' \sim q$ coordinates
v	Elasticity	Poisson's ratio
κ		Slope of the unloading line
λ	Plasticity	Slope of RNCL in $e \sim \ln p'$ coordinates
N		e at $p' = 1$ kPa for RNCL
Z		e at $p' = 1$ kPa for NCL
χ	Dilatancy	Control the size of dilatancy
m		Control the rate of dilatancy

Symbol	Equation	Description
Intermediate variables		
E	$E = \frac{3(1-2v)(1+e_0)}{\kappa}(p' + p_s)$	Elastic modulus
M_c	$M_c = M \cdot \exp(-m \cdot \xi)$	Characteristic state stress ratio
M_f	$M_f = 6\left(\sqrt{\frac{12(3-M)}{M^2}\exp\left(-\frac{\xi}{\lambda-\kappa}\right) + 1} + 1\right)^{-1}$	Potential failure stress ratio
ξ	$\xi = \Delta e_{EB} = Z - \lambda \ln\left(\frac{p' + p_s}{1 + p_s}\right) - (\lambda - \kappa)\ln\left(\frac{\left(\frac{M^2+\eta^2}{M^2-\chi\eta^2}\right)p' + p_s}{p' + p_s}\right) - e$	State variable
p_s	$p_s = \exp\left(\frac{N-Z}{\lambda}\right) - 1$	Compressive hardening parameter
c_p	$c_p = \frac{\lambda-\kappa}{1+e_0}$	Plastic coefficient

In the case of clay materials, Z equals N, resulting in only seven parameters

Recently, the original UH model is further extended for granular materials [48], which is the so-called CSUH model.

The CSUH model can degrade into the original UH model for overconsolidated clays and can further degrade into the MCC model for normally consolidated clays [48]. Therefore, the highlights of the CSUH model can be appreciated by comparing its basic features with the MCC model, as shown in Table 1. The parameters of the CSUH model as well as some intermediate variables are summarized in Table 2. In the following, a brief review of the CSUH model is outlined:

1. *Basic framework*. The CSUH model extends the isotropic normal compression line (NCL) of the MCC model to a more generalized form for sands. The new NCL becomes a curved line by introducing a new interception Z. In the CSUH model, the NCL of the MCC model is called the reference normal compression line (RNCL). The NCL of the CSUH model asymptotically approaches the RNCL when the parameter Z is equal to N. In addition, the CSUH model indicates that the current state of point B is not necessarily unloaded from an isotropic compression line, as proposed by the MCC, but may be from a more generalized anisotropic compression line (ACL). As illustrated in Figs (a) and (b) of Table 1, the ACL is defined by the parameters Z and χ.
2. *Plastic potential*. The MCC model adopts the associated flow rule, while the CSUH model adopts the non-associated flow rule. The parameter M in the plastic potential equation of the MCC model is replaced by M_c in the CSUH model.
3. *Yield Function*. The CSUH model adopts a drop-shaped yield function by introducing a critical state parameter χ. This parameter can adjust the vertical distance between the NCL and the critical state line (CSL), i.e., Δe_{A_2F} shown in Fig (c) of Table 1, leading to a feasible control of the dilatancy.
4. *Hardening law*. The hardening law of the CSUH model adopts a similar form as the unified hardening parameter in the UH model for overconsolidated clay. A new dilatancy parameter m is introduced in the expression of the characteristic state stress ratio M_c to control the rate of dilatancy. The larger m is, the earlier the current

Table 3 Boundary conditions and the controlling equations of the CSUH model for modeling conventional triaxial tests

Test type	Isotropic compression test	CD test	CU test
Boundary conditions	$\Delta\sigma'_2 = \Delta\sigma'_3$ $\Delta\sigma'_1 = \Delta\sigma'_2 = \Delta\sigma'_3$	$\Delta\sigma'_2 = \Delta\sigma'_3 = 0$	$\Delta\varepsilon_1 + \Delta\varepsilon_2 + \Delta\varepsilon_3 = 0$
Controlling equations	$\left.\begin{array}{l} \Delta\sigma'_1 = \dfrac{\Delta\varepsilon_1}{C_{11}+C_{12}+C_{13}} \\ \Delta\sigma'_2 = \Delta\sigma'_1 \\ \Delta\sigma'_3 = \Delta\sigma'_2 \\ \Delta\varepsilon_2 = (C_{21}+C_{22}+C_{23})\Delta\sigma'_1 \\ \Delta\varepsilon_3 = \Delta\varepsilon_2 \end{array}\right\}$	$\left.\begin{array}{l} \Delta\sigma'_1 = \dfrac{\Delta\varepsilon_1}{C_{11}} \\ \Delta\sigma'_2 = 0 \\ \Delta\sigma'_3 = \Delta\sigma'_2 \\ \Delta\varepsilon_2 = C_{21}\Delta\sigma'_1 \\ \Delta\varepsilon_3 = \Delta\varepsilon_2 \end{array}\right\}$	$\left.\begin{array}{l} \Delta\sigma'_1 = \dfrac{\Delta\varepsilon_1}{C_{11} - \left(\frac{(C_{11}+C_{21}+C_{31})(C_{12}+C_{13})}{C_{13}+C_{23}+C_{33}+C_{12}+C_{22}+C_{32}}\right)} \\ \Delta\sigma'_2 = \dfrac{-(C_{11}+C_{21}+C_{31})\Delta\sigma'_1}{C_{13}+C_{23}+C_{33}+C_{12}+C_{22}+C_{32}} \\ \Delta\sigma'_3 = \Delta\sigma'_2 \\ \Delta\varepsilon_2 = C_{21}\Delta\sigma'_1 + (C_{22}+C_{23})\Delta\sigma'_3 \\ \Delta\varepsilon_3 = \Delta\varepsilon_2 \end{array}\right\}$

stress ratio η exceeds the current M_c, leading to volume dilation.

As shown in Table 2, the CSUH model involves eight basic material parameters, with the first five being the same with the MCC and the original UH models [44, 48]. The CSUH model can degrade to the original UH model by setting parameter $Z = N$ and by setting parameters χ and m to be zero. Due to this feature, the CSUH model is able to uniformly decipher the mechanical behaviors of both clays and sands. For details regarding the formulation and prediction performance of the CSUH model, the reader may refer to the literature [48].

2.2 Numerical integration

The CSUH model is an incrementally elastoplastic model which requires step-by-step integrations for establishing the stress–strain and excess pore pressure relationships, as follows:

$$\{\Delta\varepsilon_i\} = \left[C_{ij}\right]\left\{\Delta\sigma'_j\right\}, \quad i = 1, 2, 3, \quad j = 1, 2, 3 \tag{1}$$

where $\left[C_{ij}\right]$ represents the elastoplastic matrix $\left[C_{ij}^{\text{ep}}\right]$ during loading process and elastic matrix $\left[C_{ij}^{\text{e}}\right]$ during unloading

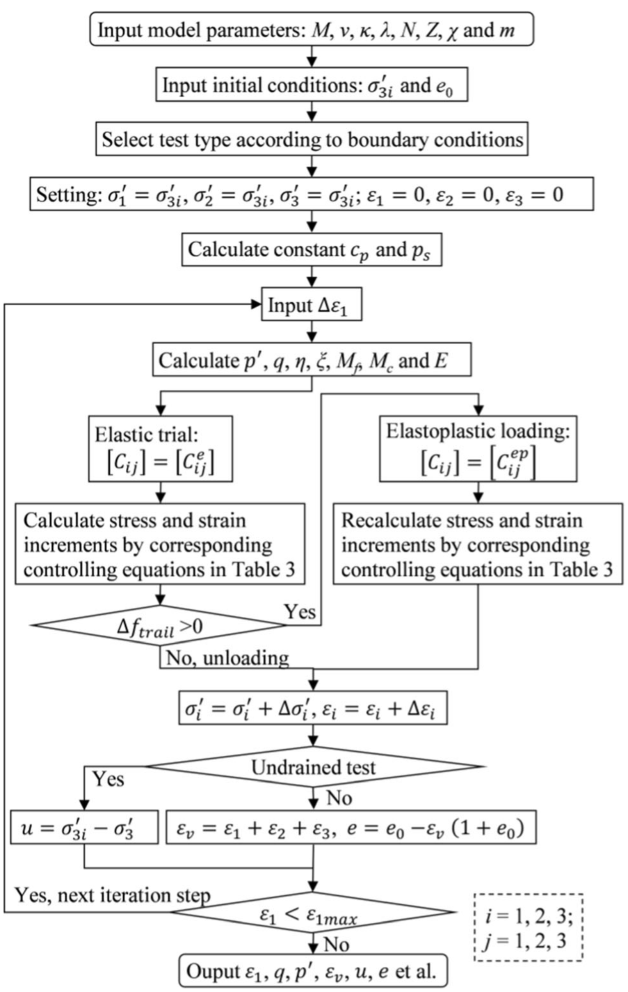

Fig. 1 Flowchart of the iterative process of the CSUH model in triaxial tests

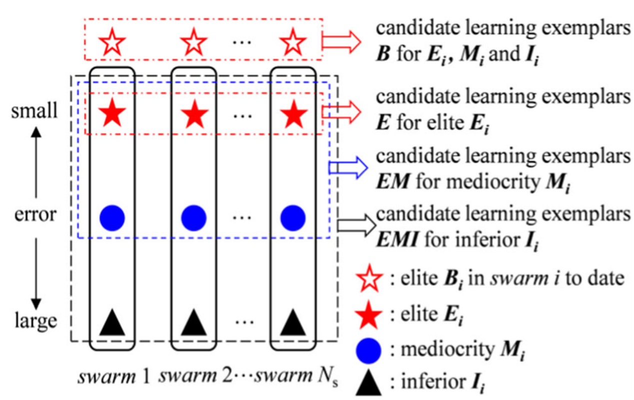

Fig. 2 Candidate learning exemplars for different exemplars X_i in each generation

process, i.e., elastic process. The elastoplastic matrix $\left[C_{ij}^{ep}\right]$ is defined as

$$\left[C_{ij}^{ep}\right] = \left[C_{ij}^{e}\right] + \left[C_{ij}^{p}\right] \tag{2}$$

with

$$\left[C_{ij}^{e}\right] = \frac{1}{E}\begin{bmatrix} 1 & -v & -v \\ -v & 1 & -v \\ -v & -v & 1 \end{bmatrix}, \tag{3}$$

and

$$\left[C_{ij}^{p}\right] = c_p \frac{M_c^4 - \eta^4 \frac{\partial f}{\partial \sigma_j'}}{M_f^4 - \eta^4 \frac{\partial g}{\partial p'}} \frac{\partial g}{\partial \sigma_i'}, \quad i = 1,2,3, \quad j = 1,2,3 \tag{4}$$

being the elastic and plastic matrixes, respectively. $\left[C_{ij}^{e}\right]$ can be obtained from the elastic modulus E varying with mean effective stress p' and Poisson's ratio v. The plastic matrix $\left[C_{ij}^{p}\right]$ can then be obtained from intermediate variables listed in Table 2 and the partial derivative formulas in the literature [48].

The numerical integration in a conventional triaxial test can be started with the input of the axial strain increments $\Delta\varepsilon_1$ and gives the output of the principal stress increments ($\Delta\sigma_1'$, $\Delta\sigma_2'$ and $\Delta\sigma_3'$) and the lateral principal strain increments ($\Delta\varepsilon_2$ and $\Delta\varepsilon_3$). The boundary conditions and the controlling equations are listed in Table 3.

The loading–unloading criterion is expressed by the following elastic trial function in which the principal stress increments are calculated using the elastic matrix.

$$\Delta f_{\text{trial}} = \frac{\partial f}{\partial \sigma_1'}\Delta\sigma_1' + \frac{\partial f}{\partial \sigma_2'}\Delta\sigma_2' + \frac{\partial f}{\partial \sigma_3'}\Delta\sigma_3' \tag{5}$$

The above criterion indicates that with a positive Δf_{trial}, the numerical step is a loading process during which the principal stress increments and lateral principal strain increments need to be recalculated by the elastoplastic matrix; otherwise, the step is an unloading process. With the model parameters, boundary conditions, and controlling equations, the stress–strain and strain-pore pressure relationships in conventional triaxial tests can be calculated according to the flowchart in Fig. 1.

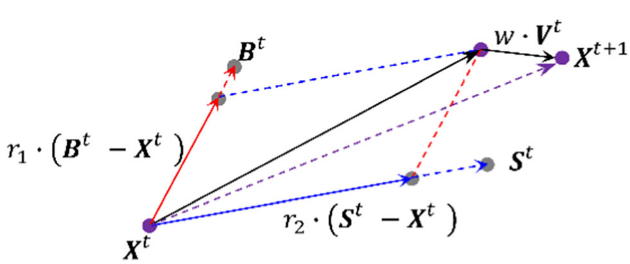

Fig. 3 The method of updating exemplars X^{t+1} in the MAPSO algorithm

3 The particle swarm optimization algorithm

3.1 Framework of the swarm population

The canonical particle swarm optimization (PSO) algorithm was originally developed by Kennedy and Eberhart to optimize nonlinear functions and train the neural network [11, 3]. To better balance the exploration (global search) and exploitation (local search) capabilities, Wei et al. [40] proposed a PSO variant based on multiple adaptive strategies (MAPSO), which has a promising performance on complicated problems. Thus, the MAPSO is adopted to calibrate parameters of constitutive model in this study. MAPSO divides all the exemplars, i.e., particles, in the canonical PSO algorithm into N_s swarms, and then different exemplars X_i can automatically select their learning exemplars (ALE) to improve their diversity.

As shown in Fig. 2, the exemplars are contained in matrices with the following definitions:

Swarm: A swarm consists of three exemplars arranged in columns. Based on error value, the three exemplars in a swarm are categorized into elite $\boldsymbol{E}_i$, mediocrity $\boldsymbol{M}_i$, and inferior $\boldsymbol{I}_i$, among which the elite exemplar has the least error.

Population matrix $\boldsymbol{\Gamma}$*:* This matrix is organized by N_s swarms. It includes all the exemplars with number of $N_1 = 3 \times N_s$.

"*Best so far*" *matrix* $\boldsymbol{B}$: This is a vector consisting of N_s elements out of the population matrix, and each represents the best elite exemplar of the swarm to date with the same column. The elements are denoted by $\boldsymbol{B}_1, \boldsymbol{B}_2, \ldots, \boldsymbol{B}_{Ns}$. The exemplar B_i is the first candidate learning exemplars of $\boldsymbol{E}_i$, $\boldsymbol{M}_i$ and $\boldsymbol{I}_i$.

Submatrices ***E****,* ***EM*** and ***EMI***: These submatrices are defined for picking up the second candidate learning exemplars of $\boldsymbol{E}_i$, $\boldsymbol{M}_i$ and $\boldsymbol{I}_i$.

The optimization algorithm will proceed with N_1 loops in each generation. Each generation updates all the exemplars in the population matrix that will be renewed

Table 4 The upper and lower boundaries of the parameters

Parameters	M	v	κ	λ	N	Z	χ	m
$\boldsymbol{R}_u$	1.8	0.45	0.1	0.4	3.0	1.5	0.99	15
$\boldsymbol{R}_l$	0.8	0.05	0.002	0.02	0.17	0.17	0.0	0.0

R_u and R_l represent the upper and lower limits of the search area

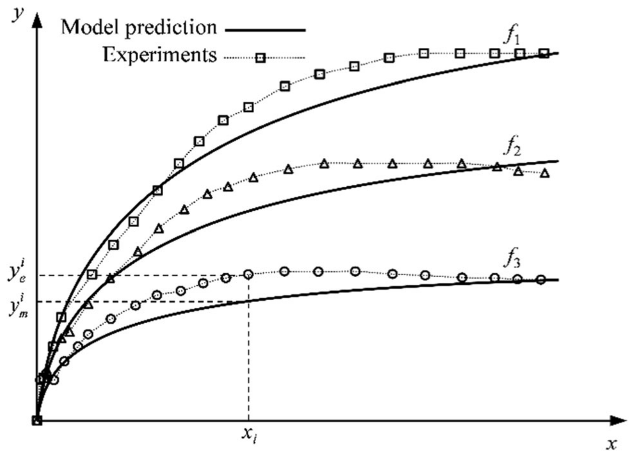

Fig. 4 The individual error of a single curve f_i

according to the rules of arrangement that have elite, mediocre and inferior exemplars sorted and rearranged based on their error values. In addition, to rationally utilize the computational resource, the MAPSO algorithm adopts an adaptive adjustment for population size (APS) by deleting or adding exemplars according to the generation that the error value of the best exemplar remains unchanged.

3.2 The process of the MAPSO algorithm

The MAPSO algorithm proceeds mainly according to the following procedures:

Step 1: The initial exemplar $\boldsymbol{X}_i$ is given randomly in the search area $\boldsymbol{R}$, and the initial velocity $\boldsymbol{V}_i$ is given randomly in the interval $[-(\boldsymbol{R}_u - \boldsymbol{R}_l)/5, (\boldsymbol{R}_u - \boldsymbol{R}_l)/5]$ with $\boldsymbol{R}_u$ and $\boldsymbol{R}_l$ being the upper and lower limits of $\boldsymbol{R}$. After filling up in the population matrix $\boldsymbol{\Gamma}$ by the N_1 number of exemplars, their error values are calculated as: $\Lambda_i = f(\mathbf{X}_i)$, $i = 1, 2, \ldots, N_1$.

Step 2: Sort the swarms in the population matrix based on their values of Λ. The population matrix thus looks like Fig. 2, which arranges the exemplars in ascending order arranged by inferior, mediocre and elite elements.

Step 3: Update the candidate learning exemplars in the "*best so far*" vector by making $\boldsymbol{B}_i = \boldsymbol{E}_i$, $i = 1, 2,\ldots, N_s$, which is the first generation of candidate learning exemplars that have relatively small values of Λ.

Step 4: Generate a new population matrix with

$$\mathbf{X}^{t+1} = \mathbf{X}^t + \mathbf{V}^{t+1} \tag{6}$$

where $\mathbf{V}^{t+1}$ is a velocity of an exemplar expressed as follows:

$$\mathbf{V}^{t+1} = w \cdot \mathbf{V}^t + r_1 \cdot (\mathbf{B}^t - \mathbf{X}^t) + r_2 \cdot (\mathbf{S}^t - \mathbf{X}^t) \tag{7}$$

The superscripts t and $t + 1$ represent the numbers of this generation and the next generation, respectively. In this equation, the first candidate learning exemplar $\boldsymbol{B}^t$ is the elite exemplar belonging to the same swarm of $\boldsymbol{X}^t$. As shown in Fig. 2, $\boldsymbol{S}^t$ is the second candidate learning exemplar randomly taken from submatrices $\boldsymbol{E}$, $\boldsymbol{EM}$, or $\boldsymbol{EMI}$ if $\boldsymbol{X}^t$ is attributed to elite, mediocrity and inferior, respectively. This process of automatically selecting two candidate learning exemplars for a given exemplar is called ALE. w represents an inertia weight denoting how much the previous velocity is preserved and is equal to 0.9–0.8 × t/t_m, where t_m represents the maximum numbers of generation; and r_1 and r_2 are two random numbers uniformly distributed in the interval [0, 1]. The operation process of updating each exemplar in the population matrix by two candidate learning exemplars can be represented by a vector operation diagram, as shown in Fig. 3.

Step 5: Repeat step 2 for sorting the new population matrix and Step 3 for renewing the "*best so far*" matrix.

Step 6: Delete or add exemplars according to APS.

Step 7: Repeat Step 4 for a new round of generation until the loop time t reaches a preset limit t_m.

Step 8: Select the one with the least error from $\boldsymbol{B}_i$ as the optimal output.

3.3 The optimization statements

The optimization for calibrating the CSUH model proceeds using the following definitions:

Exemplar: A vector containing the basic parameters represented by $\boldsymbol{X} = (M, v, \kappa, \lambda, N, Z, \chi, m)$ for the CSUH model.

Search area: The MAPSO algorithm requires a reasonable area defined by $\boldsymbol{R}$ for searching the optimized

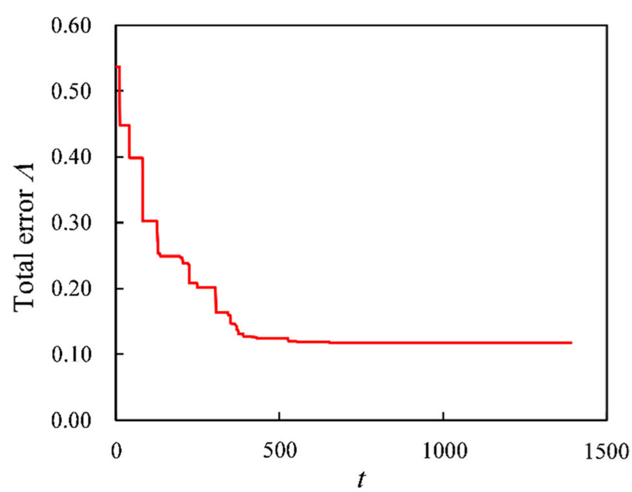

Fig. 5 The generation t versus the total error value Λ during the parameter optimization of the LCT clay

Table 5 Optimization parameters for LCT clay by MAPSO

Parameters and total error	M	v	κ	λ	N	Z	χ	m	Λ
Initial guess	1.036	0.385	0.03	0.093	0.955	0.955	0.014	3.666	0.537
Optimized result	1.235	0.449	0.004	0.059	0.745	0.745	0.229	11.406	0.117

parameters. The limits of the five parameters (M, v, κ, λ, N) are suggested by the MCC model [5, 19, 32, 33, 35, 49]. For sands, the parameter Z is close to the maximum void ratio, approximately (0.4–0.7) times of N. For clays, Z is equal to parameter N. The parameters χ and m lie, respectively, in the ranges of [0, 1) and $[0,\ (1-\chi)/[(\lambda-\kappa)(1+\chi)])$ [48]. Table 4 gives the suggested upper and lower boundaries of the parameters for the CSUH model.

Individual error: The following two criteria are used for assessing the relative errors between the experimental data and model prediction [2].

Mean relative error

$$MRE = \frac{1}{N_2}\sum_{i=1}^{N_2}\frac{\left|y_e^i(x_i) - y_m^i(x_i)\right|}{\left|y_e^i(x_i)\right|} \tag{8}$$

Determination coefficient

$$R = 1 - \sqrt{\frac{\sum_{i=1}^{N_2}\left(y_e^i(x_i) - y_m^i(x_i)\right)^2}{\sum_{i=1}^{N_2}\left(y_e^i(x_i)\right)^2}} \tag{9}$$

where $y_e^i(x_i)$ and $y_m^i(x_i)$ represent the ith experimental and model-predicted y with the same x_i, respectively, as shown in Fig. 4. N_2 is the total number of experimental points in a single curve, MRE represents the relative difference between the experimental data and model prediction, and R describes the analogy in the distribution tendency of the two datasets. In this study, we set $MRE < 0.2$ and $R > 0.85$ as the criteria for an acceptable prediction. In the parameter optimization of CSUH, y represents the variables q, p', ε_v, u or e, while x represents ε_1.

It should be noted that the two criteria have a limitation when the values of $y_e^i(x_i)$ are close to zero, making the denominators of Eqs. (8) and (9) close to zero as well. The errors calculated by them are therefore exaggerated. On this occasion, these criteria may not be applicable.

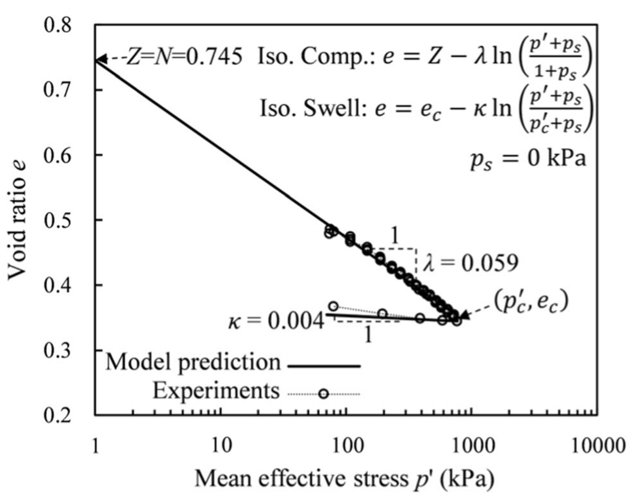

Fig. 6 Comparisons between the isotropic compression and extension tests of LCT clay [25] and CSUH simulations in $e \sim \lg p'$ coordinates

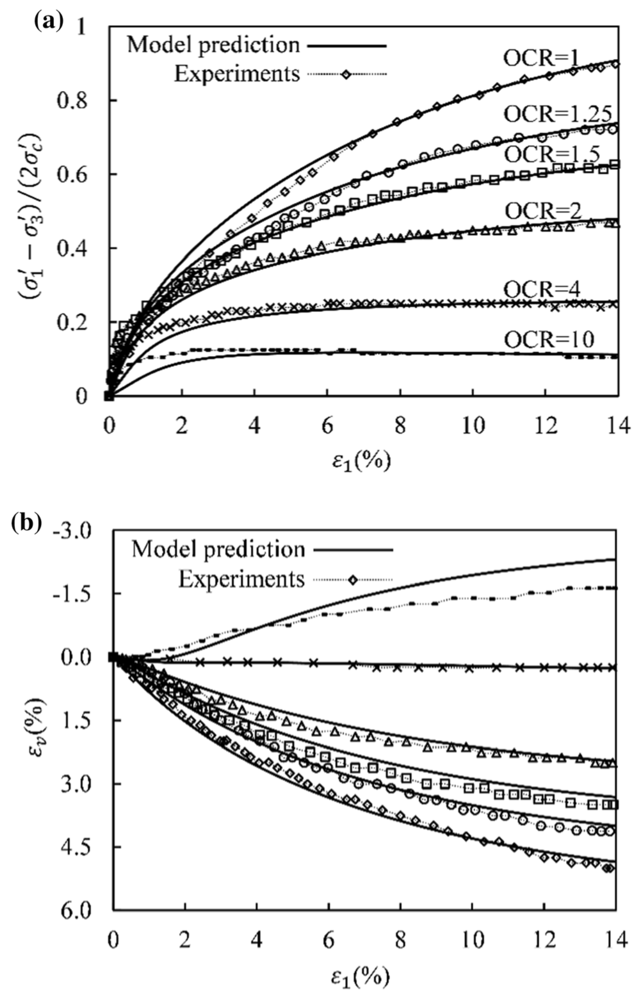

Fig. 7 Comparisons between the CD test results of LCT clay [25] and CSUH simulations: **a** axial strain versus deviatoric stress and **b** axial strain versus volumetric strain

Table 6 The *MRE* and *R* values of model prediction in CD tests on the LCT clay

OCR		1	1.25	1.5	2	4	10
$(\sigma_1' - \sigma_3')/(2\sigma_c')$	*MRE*	0.082	0.056	0.073	0.073	0.124	0.155
	R	0.944	0.952	0.949	0.925	0.878	0.822
ε_v	*MRE*	0.062	0.142	0.126	0.107	0.065	0.635
	R	0.958	0.949	0.918	0.923	0.932	0.635

Total error: Suppose there are altogether N_3 comparisons between the experimental data and model prediction, as shown in Fig. 4 (here $N_3 = 3$), whose mean relative errors are MRE_j, $j = 1, 2,\ldots, N_3$. The total error Λ is defined as their average value.

$$\Lambda = \frac{1}{N_3}\sum_{j=1}^{N_3} MRE_j \tag{10}$$

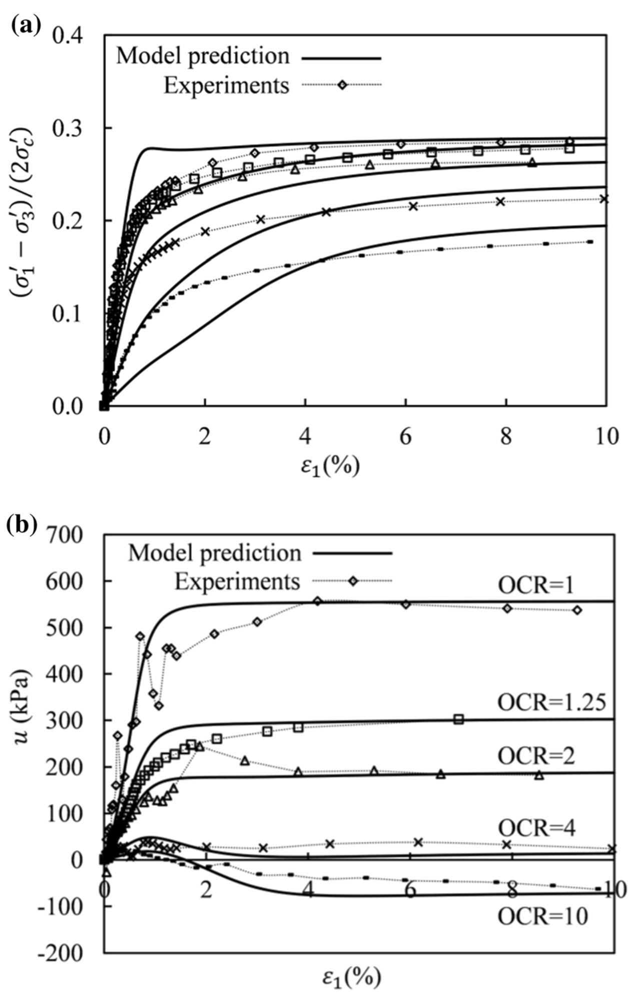

Fig. 8 Comparisons between the CU test results of LCT clay [25] and the CSUH predictions: **a** axial strain versus deviatoric stress and **b** axial strain versus excess pore pressure

Obviously, a smaller total error indicates a better fitting exemplar. For N_3 relationships $y_j = f_j(\boldsymbol{X})$, $j = 1, 2,\ldots, N_3$, find the $\boldsymbol{X}$ associated with the minimum total error subject to the restriction that $\boldsymbol{X}$ is within the search area $\boldsymbol{R}$, then the optimization statement is

$$\begin{aligned} \min\ \Lambda &= f(\mathbf{X}) \\ \text{s.t.}\,\mathbf{X} &\in \mathbf{R} \end{aligned} \tag{11}$$

In this study, the investigated relationships are (1) N_3 number of axial strains versus the deviatoric stress. (2) N_3 number of axial strains versus volumetric strain and (3) one curve depicting isotropic compression. N_4 is the total number of individual errors in drained tests and is equal to $2 \times N_3 + 1$.

4 Calibration and validation

4.1 Clay material

4.1.1 Calibration

The experimental results from drained and undrained conventional triaxial compression tests on saturated Lower Cromer Till (LCT) clay were collected from Pestana et al. [25]. The LCT clay in isotropic compression test is compressed to p_c' and then unloaded with different over-consolidation ratios (OCRs). The pre-consolidation pressure p_c' (also denoted by σ_c') equals 770 kPa, and the corresponding void ratio e_c is 0.345. The isotropic compression test result is actually a part of CD tests related to the initial values of e_0 and $\ln p_0$ of the individual triaxial compression tests associated with various confining pressures p_0. In the

Table 7 Evaluation of the individual errors *MRE* and *R* in the prediction of undrained triaxial tests on the LCT clay

OCR		1	1.5	2	4	10
$(\sigma_1' - \sigma_3')/(2\sigma_c')$	*MRE*	0.048	0.035	0.083	0.086	0.135
	R	0.934	0.956	0.903	0.892	0.857
u	*MRE*	0.076	0.083	0.07	0.601	0.708
	R	0.908	0.906	0.904	0.331	0.453

Table 8 Optimization parameters for the rockfill material from the Changhe dam

Parameters and total error	M	v	κ	λ	N	Z	χ	m	Λ
Initial guess	1.710	0.189	0.082	0.090	1.152	0.432	0.233	11.004	0.202
Optimized result	1.678	0.272	0.021	0.087	1.125	0.742	0.385	1.716	0.061

consolidation stage, the isotropic compression test is carried out to obtain the initial values of e_0 and $\ln p_0$ before shearing stage of the triaxial compression tests. Thus, the isotropic compression test result is actually a part of CD tests.

The experimental data from isotropic compression test and CD test are adopted for the MAPSO algorithm to calculate the basic parameters of the CSUH model. Here, the population dimension N_1 = 75 in each generation. The best exemplar, selected from 80 × N_1 random initial exemplars, is taken as the initial guess parameter. The set of parameters that leads to the minimum total error is taken as the optimization parameter. The change in the total error value in the optimization process is shown in Fig. 5. The initial guess and final optimization parameters are given in Table 5.

In this particular case, the researchers also performed isotropic compression and extension tests for the LCT clay, from which one may gain the actual basic parameters M = 1.2, κ = 0.009, λ = 0.06 and N = Z = 0.752, as shown in Fig. 6 [25, 48]. This thus gives us an opportunity to check the performance of the calibration method. The comparisons between the actual basic parameters and the optimized parameters show that all the parameters except for κ are in good agreement. The isotropic compression test is a part of the CD test, while the isotropic extension test is not. Therefore, the isotropic extension test is not used in the back analysis of parameters, which may be the reason why the optimized κ differs greatly from the actual κ.

With the optimized parameters listed in Table 5, the mechanical response of the LCT clay can be predicted by the CSUH model. Figure 7 shows the comparison between experiments and model prediction in terms of axial strain ε_1 versus deviatoric stress q and axial strain ε_1 versus volumetric strain ε_v. The individual errors MRE and R of most prediction summarized in Table 6 meet the criteria $MRE < 0.2$ and $R > 0.85$. Only the prediction of the volumetric strain the values of relative for OCR = 10 slightly

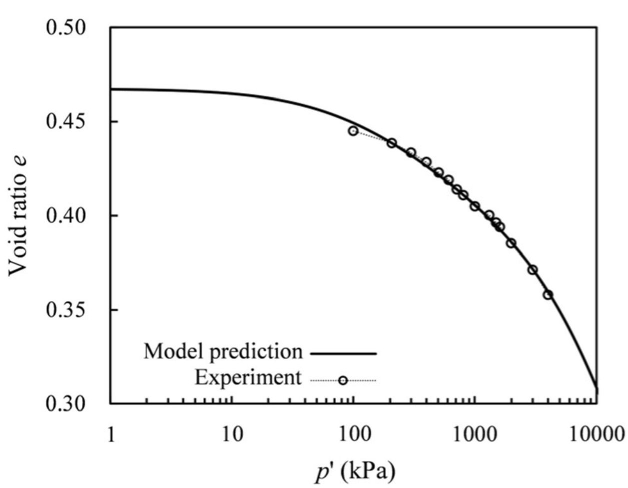

Fig. 9 Comparisons between the isotropic compression test results of the rockfill [17] and the CSUH simulations in the $e \sim \lg p'$ coordinates (MRE = 0.003, R = 0.996)

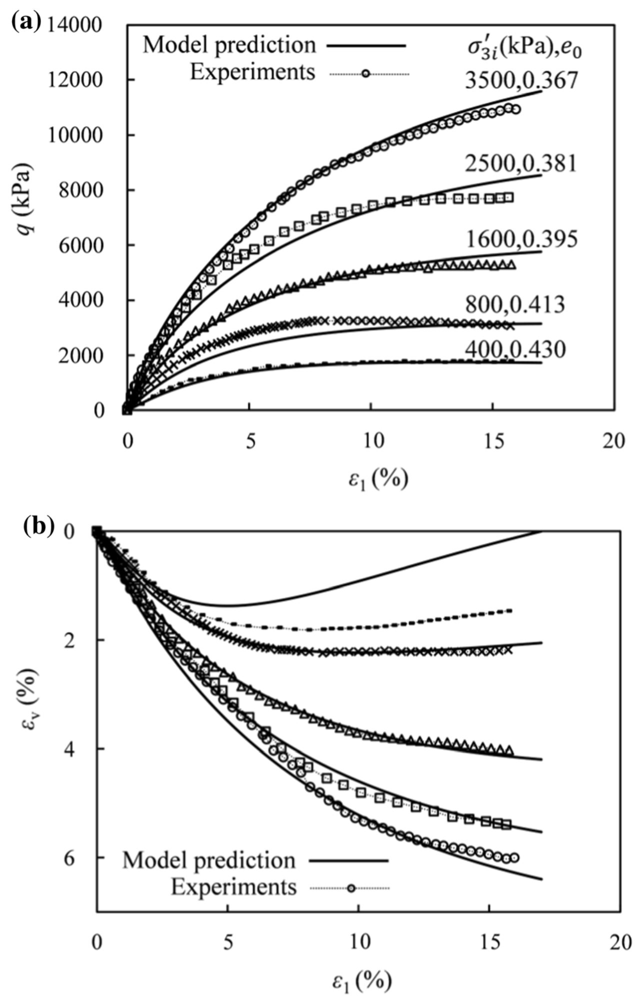

Fig. 10 Comparisons between the CD test results of the rockfill [17] and the CSUH simulations: **a** axial strain versus deviatoric stress and **b** axial strain versus volumetric strain

Table 9 Evaluation of the individual errors *MRE* and *R* in the prediction of drained triaxial tests on the rockfill

σ'_{3i} (kPa)		400	800	1600	2500	3500
q	*MRE*	0.041	0.137	0.046	0.072	0.045
	R	0.958	0.864	0.959	0.936	0.972
ε_v	*MRE*	0.450	0.051	0.021	0.033	0.064
	R	0.470	0.965	0.981	0.970	0.956

exceeds the criteria, while the absolute difference between experimental and predicted results is small. A comprehensive analysis shows that the prediction of volumetric strain is good. In general, the CSUH model gives an excellent prediction of the deviatoric stress and the volumetric strain of LCT clay in the drained test under different OCRs.

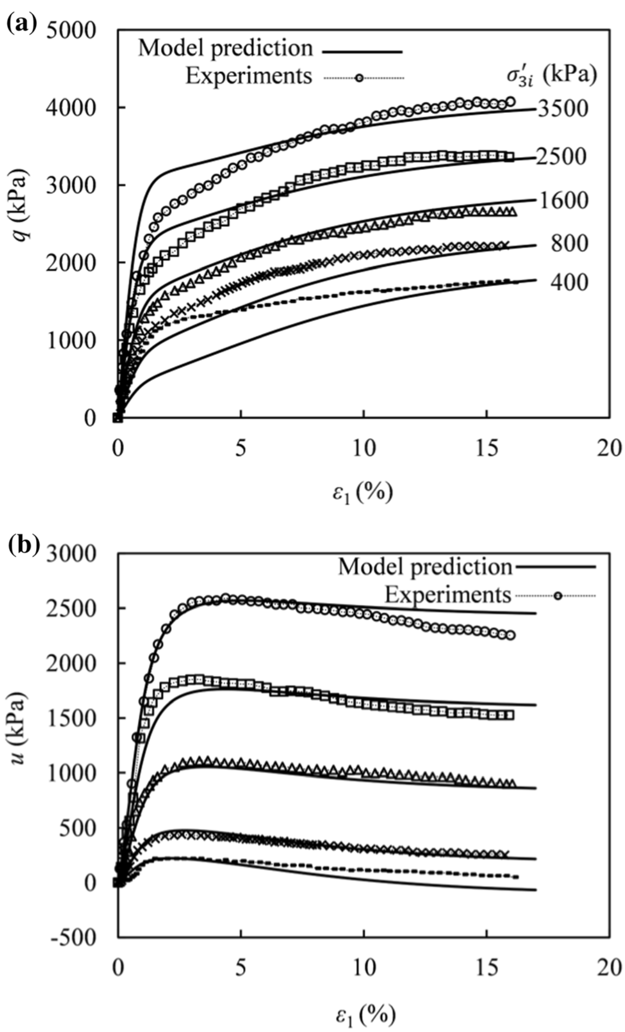

Fig. 11 Comparisons between the CU test results of the rockfill [17] and the CSUH predictions: **a** axial strain versus deviatoric stress and **b** axial strain versus excess pore pressure

4.1.2 Validation

The stress–strain relations during the undrained tests are more easily affected by the dilatancy than that in drained tests. The volumetric strain is usually smaller than the deviatoric strain during the drained shearing. Thus, if the prediction of the volumetric strain caused by the dilatancy is inaccurate, the prediction deviation of the stress–strain relations in the drained stress path is not significant. Moreover, dilatancy does not affect the stress path and the residual strength in the drained conditions; thus, it has less influence on the stress–strain relations in the drained conditions.

However, in the undrained conditions, the volumetric strain increment is zero, and there is a coupling relationship between the recoverable and the unrecoverable increments. In an undrained shearing, the unrecoverable volumetric strain increment is affected by its deviatoric component through dilatancy. Then, the unrecoverable volumetric strain increment influences the recoverable volumetric strain increment through the coupling relationship, thereby affecting the mean effective stress. The dilatancy greatly affects the effective stress path, and thus, it can significantly affect the strength of soils under undrained conditions. A slight error in the description of dilatancy under the undrained conditions may result in a sizeable stress–strain relation deviation, and the phenomenon "one false step will make a great difference" will appear. Therefore, it is essential and critical to validate the constitutive model through undrained tests.

In what follows, we will validate the CSUH model by predicting the undrained mechanical response of LCT clay using the calibrated parameters listed in Table 5. The selected experiments are related to OCR values of 1, 1.25, 2, 4, and 10. Figure 8 shows the comparisons between the experiments and prediction in terms of ε_1 versus $(\sigma'_1 - \sigma'_3)/(2\sigma'_c)$ and ε_1 versus u.

Similar to Table 6, we also calculate the relative errors *MRE* and *R* in the prediction of undrained triaxial tests on LCT clay. The total errors of the ε_1 versus $(\sigma'_1 - \sigma'_3)/(2\sigma'_c)$ relationships for all cases of OCR values are good, meeting the criteria of $MRE < 0.2$ and $R > 0.85$ as shown in Table 7. With respect to the ε_1 versus u relationship, we find that *MRE* and *R* cannot meet these two criteria for OCR = 4 and 10. A further inspection on Fig. 8b reveals that the values of u are very close to zero, making both *MRE* and *R* be exaggerated by using Eqs. (8) and (9). In general, the predictions on excess pore pressure also show good agreement with the experiments except for the case of OCR = 10 in which the values *MRE* and *R* are 0.708 and 0.453, respectively.

Table 10 Evaluation of the individual errors *MRE* and *R* in the prediction of undrained triaxial tests on the rockfill

σ'_{3i} (kPa)		400	800	1600	2500	3500
q	*MRE*	0.261	0.141	0.051	0.054	0.073
	R	0.757	0.875	0.958	0.943	0.923
u	*MRE*	0.685	0.197	0.067	0.053	0.037
	R	0.490	0.932	0.936	0.936	0.959

4.2 Granular material

4.2.1 Calibration

A further simulation is performed to examine the proposed method for calibrating and validating the CSUH model in predicting the mechanical behavior of granular materials. A saturated rockfill material from the Changhe dam (CHD) is selected for this investigation [17]. This material was thoroughly investigated by Liu et al. [17] through isotropic compression, CD, and CU tests with a high-pressure triaxial apparatus.

The model parameters for the rockfill material are calibrated using the MAPSO algorithm based on isotropic compression and CD tests. The initial and optimized results are listed in Table 8.

The simulated results of the isotropic compression test and the drained triaxial tests on the rockfill material are, respectively, shown in Figs. 9 and 10. It can be seen that the CSUH model gives rise to excellent predictions of both tests. Most of the predictions agree well with the test results and meet the criteria with $MRE < 0.2$ and $R > 0.85$ as shown in Table 9, except for the prediction of volumetric change with the confining pressure of 400 kPa, in which the *MRE* and *R* is 0.45 and 0.47, respectively. These results suggest that the CSUH model can sufficiently describe dilatancy of rockfill materials.

4.2.2 Validation

The following content is related to the validation of the CSUH model with the calibrated parameters. Likewise, the parameters listed in Table 8 are used to predict the undrained behavior. The comparisons between experiments and model prediction are shown in Fig. 11.

An inspection of Fig. 11 suggests that the numerical predictions of the relationships ε_1 versus q and ε_1 versus u in undrained triaxial tests agree well with the experimental results. Most of the predictions meet the pre-described criteria except for the tests with confining pressure of 400 kPa in which the values of *MRE* and *R* of the relationships of ε_1 versus q are 0.261 and 0.757, respectively, and the values of *MRE* and *R* of the relationships of ε_1 versus u are 0.685 and 0.490, respectively, refer to Table 10. This may be attributable to the fact that granular material may exhibit remarkable dilatancy under low level of confining pressure. In general, the CSUH model can reasonably describe the strain hardening, as well as the phenomenon that the excess pore water pressure first increases and then decreases in the undrained tests.

5 Conclusions

This paper presents a standard methodology for calibrating and validating constitutive models with conventional triaxial tests results. For this purpose, we consider a recently proposed constitutive model, the CSUH model, for clays and sands. The CSUH model is an upgrade in theory and innovative development of the modified Cam-Clay model. By introducing the compressive hardening parameter p_s, the CSUH model can describe the compressive hardening characteristics of both sands and clays. In addition, the CSUH model adopts the same hardening law of the original UH mode, which is able to capture dilatancy and strain softening behaviors of overconsolidated soils. By combing all the features in a single framework, the CSUH model is able to sufficiently decipher the mechanical behaviors of various soils (e.g., clays, sands, and rockfill materials, etc.) in a uniform way, which is exactly what Wroth and Houlsby expected [42].

It is believed that verifying the CSUH model with the independent tests can increase the credibility of this research. With the help of the MAPSO algorithm, the parameters of the CSUH model can be calibrated through drained triaxial compression tests on clay and rockfill materials. The accuracy of the optimization is examined by two relative errors. Furthermore, the CSUH model with the calibrated parameters is validated by simulating undrained triaxial compression tests. The prediction shows an excellent agreement with the experimental results. In general, the results demonstrate that the CSUH model has a strong ability for predicting the mechanical behavior of various soils.

Acknowledgements This study was supported by the National Key R&D Program of China (Grant No. 2018YFE0207100), the National Natural Science Foundation of China (Grant No. 51979001), and the National Key Basic Research Development Plan of China (Grant No. 2014CB047006). Thanks to Professor Enlong Liu for the discussion and experimental data. Thanks to Professor Xuewen Xia for providing the source code of the MAPSO algorithm. Thanks to Professor Erxiang Song and Xu Li for their valuable advice. Thanks to Dr. Shun Wang, Jian Han and Wenjie Cui for the excellent correction and polishing to this manuscript.

Funding National Key R&D Program of China (Grant No. 2018YFE0207100), Innovative Research Group Project of the

National Natural Science Foundation of China (Grant No. 51979001), National Basic Research Program of China (973 Program) (Grant No. 2014CB047006).

References

1. Calvello M, Finno RJ (2004) Selecting parameters to optimize in model calibration by inverse analysis. Comput Geotechn 31(5):410–424
2. Chen ZY, Zhang YP, Li JB, Li X, Jing LJ (2021) Diagnosing tunnel collapse sections based on TBM tunneling big data and deep learning: a case study on the Yinsong Project, China. Tunnel Undergr Space Technol 108:103700. https://doi.org/10.1016/j.tust.2020.103700
3. Eberhart R, Kennedy J A new optimizer using particle swarm theory. In: MHS'95. Proceedings of the sixth international symposium on micro machine and human science, 1995. IEEE, pp 39–43
4. Gao ZW, Zhao JD, Li XS, Dafalias YF (2014) A critical state sand plasticity model accounting for fabric evolution. Int J Numer Anal Methods Geomech 38(4):370–390
5. Gercek H (2007) Poisson's ratio values for rocks. Int J Rock Mech Min Sci 44(1):1–13. https://doi.org/10.1016/j.ijrmms.2006.04.011
6. Gras JP, Sivasithamparam N, Karstunen M, Dijkstra J (2017) Strategy for consistent model parameter calibration for soft soils using multi-objective optimisation. Comput Geotechn 90:164–175
7. Han J, Yin Z-Y, Dano C, Hicher P-Y (2021) Cyclic and creep combination effects on the long-term undrained behavior of overconsolidated clay. Acta Geotech 16(4):1027–1041
8. Han J, Yin Z-Y, Dano C, Hicher P-Y (2021) Effect of strain rate on the adhesive bond shearing resistance of stiff clay. Transp Geotechn 27:100479
9. Hashiguchi K, Chen ZP (1998) Elastoplastic constitutive equation of soils with the subloading surface and the rotational hardening. Int J Numer Anal Methods Geomech 22(3):197–227
10. Holland JH (1992) Adaptation in natural and artificial systems: an introductory analysis with applications to biology, control, and artificial intelligence. MIT Press, London
11. Kennedy J, Eberhart R (1995) Particle swarm optimization. In: Proceedings of ICNN'95-international conference on neural networks. IEEE, pp 1942–1948
12. Lade PV (1977) Elasto-plastic stress-strain theory for cohesionless soil with curved yield surfaces. Int J Solids Struct 13(11):1019–1035
13. Lade PV, Duncan JM (1975) Elastoplastic stress–strain theory for cohesionless soil. J Geotech Eng Div 101(10):1037–1053
14. Lade PV, Kim MK (1995) Single hardening constitutive model for soil, rock and concrete. Int J Solids Struct 32(14):1963–1978. https://doi.org/10.1016/0020-7683(94)00247-t
15. Lade PV (2005) Overview of constitutive models for soils. In: Soil constitutive models: Evaluation, selection, and calibration, pp 1–34
16. Levasseur S, Malécot Y, Boulon M, Flavigny E (2008) Soil parameter identification using a genetic algorithm. Int J Numer Anal Methods Geomech 32(2):189–213
17. Liu EL, Tan YL, Chen SS, Li GY (2012) Investigation on critical state of rockfill materials. J Hydraul Eng 43(5):505–511 **(in Chinese)**
18. Luo T, Chen D, Yao YP, Zhou AN (2020) An advanced UH model for unsaturated soils. Acta Geotech 15(1):145–164. https://doi.org/10.1007/s11440-019-00882-y
19. Marto A, Tan CS, Makhtar AM, Kung Leong T (2014) Critical state of sand matrix soils. Sci World J 2014
20. Matsuoka H, Yao YP, Sun DA (1999) The Cam-Clay models revised by the SMP criterion. Soils Found 39(1):81–95
21. Nakai T (1989) An isotropic hardening elastoplastic model for sand considering the stress path dependency in three-dimensional stresses. Soils Found 29(1):119–137
22. Nakai T, Matsuoka H (1986) A generalized elastoplastic constitutive model for clay in three-dimensional stresses. Soils Found 26(3):81–98
23. Pal S, Wathugala GW, Kundu S (1996) Calibration of a constitutive model using genetic algorithms. Comput Geotechn 19(4):325–348
24. Papon A, Riou Y, Dano C, Hicher PY (2012) Single-and multi-objective genetic algorithm optimization for identifying soil parameters. Int J Numer Anal Methods Geomech 36(5):597–618
25. Pestana JM, Whittle AJ, Gens A (2002) Evaluation of a constitutive model for clays and sands: Part II–clay behaviour. Int J Numer Analy Methods Geomech 26(11):1123–1146
26. Pestana JM, Whittle AJ, Salvati LA (2002) Evaluation of a constitutive model for clays and sands: part I–sand behaviour. Int J Numer Anal Methods Geomech 26(11):1097–1121
27. Roscoe K, Schofield A, Thurairajah A (1963) Yielding of clays in states wetter than critical. Geotechnique 13(3):211–240
28. Roscoe KH, Burland JB (1968) On the generalized stress–strain behaviour of 'wet clay'. In: Heyman J, Leckie FA (eds) Engineering plasticity. Cambridge University Press, Cambridge
29. Roscoe KH (1963) Mechanical behaviour of an idealized 'wet' clay. Proc 3rd Eur Conf Soil Mech Wiesbaden 1:47–54
30. Russell AR, Khalili N (2004) A bounding surface plasticity model for sands exhibiting particle crushing. Can Geotech J 41(6):1179–1192
31. SadoghiYazdi J, Kalantary F, SadoghiYazdi H (2012) Calibration of soil model parameters using particle swarm optimization. Int J Geomech 12(3):229–238
32. Schofield A, Wroth P (1968) Critical state soil mechanics. McGraw-hill, London
33. Soleimanbeigi A (2013) Undrained shear strength of normally consolidated and overconsolidated clays from pressuremeter tests: a case study. Geotechn Geol Eng 31(5):1511–1524
34. Sun DA, Sheng DC, Sloan SW (2007) Elastoplastic modelling of hydraulic and stress–strain behaviour of unsaturated soils. Mech Mater 39(3):212–221
35. Tekeste MZ, Habtzghi DH, Koolen J (2013) Cap-hardening parameters of Cam-Clay model variations with soil moisture content and shape-restricted regression model. Agric Eng Int CIGR J 15(2):10–24
36. Ti KS, Huat BB, Noorzaei J, Jaafar MS, Sew GS (2009) A review of basic soil constitutive models for geotechnical application. Electron J Geotech Eng 14:1–18
37. Wang S, Wu W (2021) A simple hypoplastic model for overconsolidated clays. Acta Geotech 16(1):21–29
38. Wang S, Wu W (2021) Validation of a simple hypoplastic constitutive model for overconsolidated clays. Acta Geotech 16(1):31–41
39. Wang S, Wu W, Zhang D, Kim JR (2020) Extension of a basic hypoplastic model for overconsolidated clays. Comput Geotechn 123:103486
40. Wei B, Xia XW, Yu F, Zhang YL, Xu X, Wu HR, Gui L, He GL (2020) Multiple adaptive strategies based particle swarm optimization algorithm. Swarm Evolut Comput 57:100731
41. Whittle A (1993) Evaluation of a constitutive model for overconsolidated clays. Geotechnique 43(2):289–313
42. Wroth C, Houlsby G (1985) Soil mechanics-property characterization and analysis procedures, UK

43. Yao YP, Feng X, Huang X, Li CL (2010) Application of UH model to finite element analysis. Rock Soil Mech 31(1):237–245 (**in Chinese**)
44. Yao YP, Gao ZW, Zhao JD, Wan Z (2012) Modified UH model: constitutive modeling of overconsolidated clays based on a parabolic Hvorslev envelope. J Geotechn Geoenviron Eng 138(7):860–868
45. Yao YP, Hou W, Zhou AN (2008) Constitutive model for overconsolidated clays. Sci China Ser E Technol Sci 51(2):179–191
46. Yao YP, Hou W, Zhou AN (2009) UH model: three-dimensional unified hardening model for overconsolidated clays. Géotechnique 59(5):451–469. https://doi.org/10.1680/geot.2007.00029
47. Yao YP, Kong LM, Zhou AN, Yin JH (2015) Time-dependent unified hardening model: three-dimensional elastoviscoplastic constitutive model for clays. J Eng Mech 141(6):04014162
48. Yao YP, Liu L, Luo T, Tian Y, Zhang JM (2019) Unified hardening (UH) model for clays and sands. Comput Geotech 110:326–343. https://doi.org/10.1016/j.compgeo.2019.02.024
49. Yao YP, Lu DC, Zhou AN, Zou B (2004) Generalized non-linear strength theory and transformed stress space. Sci China Ser E: Technol Sci 47(6):691–709
50. Yao YP, Sun DA, Matsuoka H (2008) A unified constitutive model for both clay and sand with hardening parameter independent on stress path. Comput Geotechn 35(2):210–222
51. Yao YP, Zhou AN (2013) Non-isothermal unified hardening model: a thermo-elasto-plastic model for clays. Géotechnique 63(15):1328–1345
52. Yao YP, Deng N, Liu L, Shu WJ, He G (2017) Application of the UH Model into Settlement Prediction of Rockfill Dam. 15th IACMAG
53. Yao YP, Huang J, Zhang K, Cui GZ (2020) Numerical back-analysis of creep settlement of airport high fill. Rock Soil Mech 41 (10):3395–3404+3414. https://doi.org/10.16285/j.rsm.2020.0402(**in Chinese**)
54. Yin ZY, Jin YF, Shen JS, Hicher PY (2018) Optimization techniques for identifying soil parameters in geotechnical engineering: comparative study and enhancement. Int J Numer Anal Methods Geomech 42(1):70–94
55. Zhao XL, Zhu JG, Bian HB (2019) Applicability of UH model to coarse-grained soil. MATEC Web Conf 295(1):03007
56. Zhu BL, Su XX, Cao YQ, Yan FX (2020) Determining parameters of the CSUH constitutive model by genetic algorithm. Jpn Geotechn Soc Spec Publ 8(6):188–193
57. Zhu EY, Yao YP (2015) Structured UH model for clays. Transp Geotechn 3:68–79